Neutron star cooling within the equation of state with induced surface tension
S. Tsiopelas, V. V. Sagun[1]

[1]Centro de Física da UC - CFisUC, University of Coimbra, 3004-516 Coimbra, Portugal
E-mail: st.tsiop@gmail.com, violetta.sagun@uc.pt

I. Abstract

We study the thermal evolution of neutron stars described within the equation of state with induced surface tension (IST) that reproduces properties of normal nuclear matter, fulfills the proton flow constraint, provides a high-quality description of hadron multiplicities created during the nuclear-nuclear collision experiments, and is equally compatible with the constraints from astrophysical observations and the GW170817 event. The model features strong direct Urca processes for the stars above $1.91\,M_\odot$. The IST equation of state shows a very good agreement with the available cooling data, even without introducing nuclear pairing. We also analysed the effects of the singlet proton/neutron and triplet neutron pairing on the cooling of neutron stars of different mass. We demonstrate a full agreement of the predicted cooling curves with the experimental data. Moreover, the IST EoS provides a description of Cas A with both paired and unpaired matter .

II. EoS Model

We consider a multicomponent version of the quantum generalization of the equation of state (EoS) within the surface tension induced by particle interaction (IST) [1]. The IST EoS accounts for strong short range repulsion and relatively weak long-range attraction between nucleons, while electrons are treated as an ideal Fermi gas.

Similarly to the Van der Waals approximation, repulsion between the nucleons is modelled with the hard core radius. However, in the present model the excluded volume is density-dependent rather than constant. The key feature of the developed EoS is the IST coefficient which results in correct values of four virial coefficients of hard spheres and the extension of the model's causality range to densities typical of neutron stars (NSs) [1, 2].
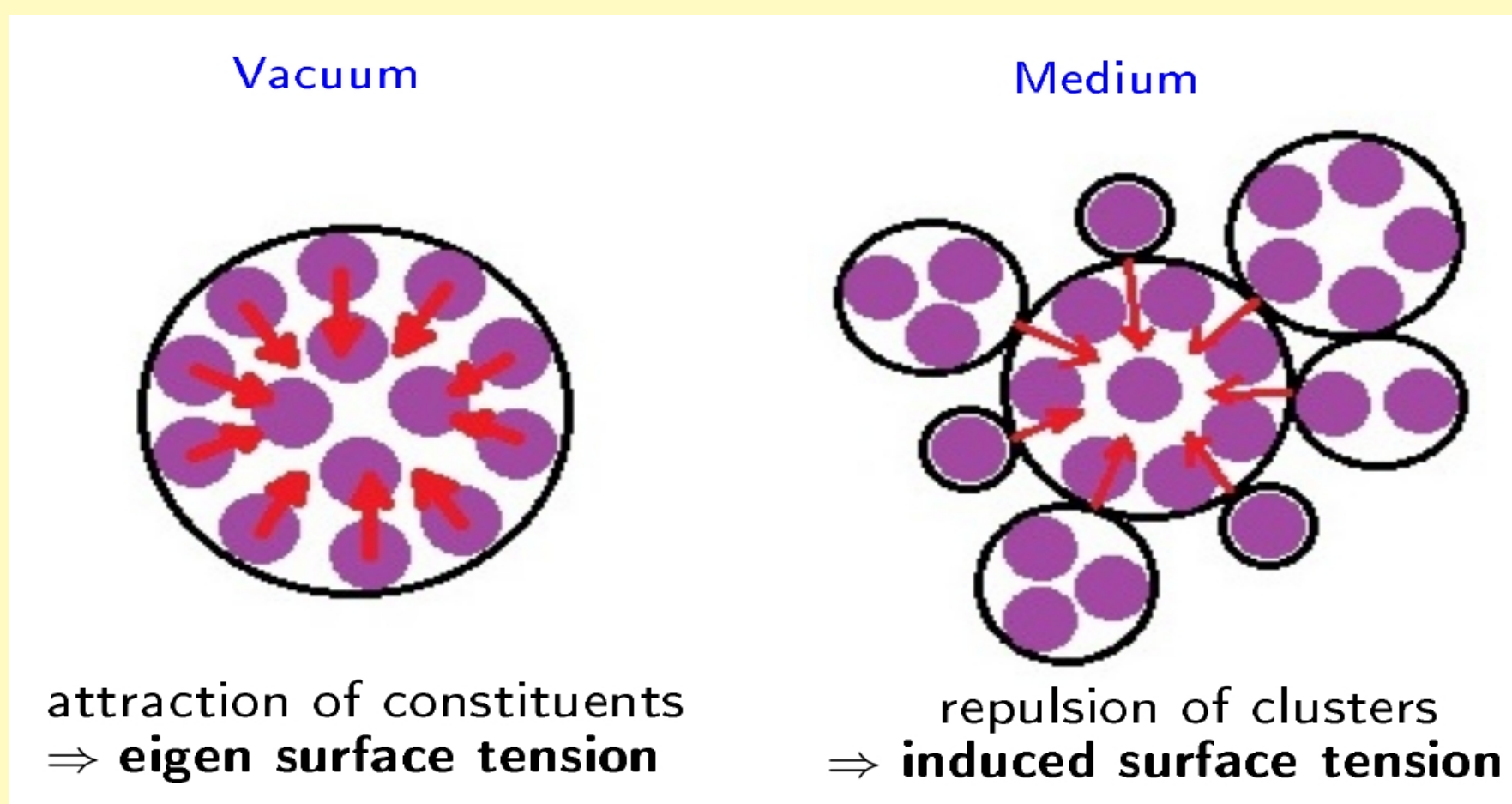

Fig.1. IST appears due to repulsion of particles in different clusters.

The long-range attraction and asymmetry between n and p are described using mean-field potentials. The associated parameters were fitted to the properties of matter at saturation density. Namely, their values at normal nuclear density are: $E_{sym} = 30.0\,MeV$, $L = 93.2\,MeV$, $K_0 = 201.0\,MeV$ for the symmetry energy, symmetry energy slope and nuclear incompressibility factor, respectively.

As shown on Fig.2, the maximum mass of the adopted EoS $M_{max} = 2.08\,M_\odot$ is consistent with the recent measurements of the most massive NSs, i.e. PSR J0348+0432 [3] and PSR J0740+6620 [4]. Moreover, the selected set of parameters is in agreement with the astrophysical constraints and results coming from the GW170817 [5]. More extensive information regarding the model and its applications to NSs can be found in Refs. [2, 6, 7].
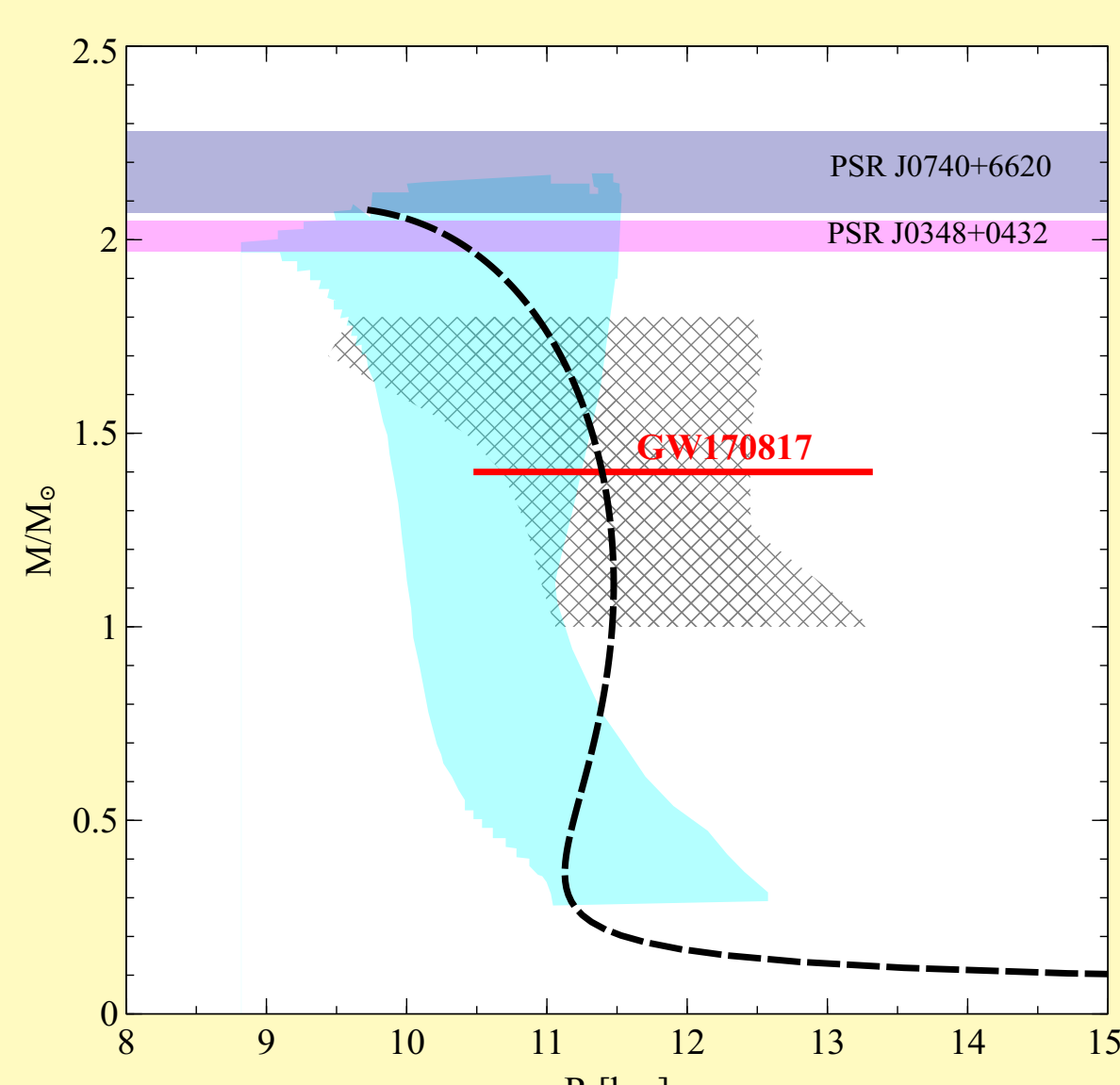

Fig.2. Mass-radius relation for non-rotating NSs calculated for the adopted IST EoS. Horizontal bands correspond to the two most massive NSs, i.e. PSR J0348+0432 [3] (magenta band) and PSR J0740+6620 [4] (blue band). The shaded grey area represents the M-R constraint taken from Refs. [8, 9], while the constraint depicted as a cyan area was taken from Ref. [10]. The red line corresponds to the the allowed range of NS radius according to the GW170817 event [5].

Acknowledgments

References

[1] Sagun, V.V. et al., Nucl. Phys. A, **924**, 24 (2014).
[2] Sagun, V.V. et al., Astrophys. J.,**871**, 157 (2019).
[3] Antoniadis, J. et al., Science, **340**, 6131, 448 (2013).
[4] Cromartie, H. T. et al., Nature Astr., **4**, 72 (2020).
[5] Abbott, B. P. et al. (LIGO and Virgo Collaborations), Phys. Rev. Lett., **119**, 161101 (2017).
[6] Sagun, V.V. et al., Nucl. Phys. A, **982**, 883 (2019).
[7] Sagun, V.V. et al., Astrophys. J., **871**, 157 (2019).
[8] Steiner, A.W. et al., Astrophys. J., **722**, 1, 33 (2010).
[9] Steiner, A.W. et al., Astrophys. J., **765**, L5 (2013).
[10] Özel, F., Freire, P., An. Rev. Astr. & Astroph. **54**, 401 (2016).
[11] Page, D. et al., Nucl. Phys. A, **777**, 497 (2006).
[12] Potekhin, A. Y., et al., Sp. Sci. Rev., **191**, 239 (2015).
[13] Potekhin, A. Y. et al., Astrophys. J., **594**, 1, 404 (2003).
[14] Bardeen, J. et al., Phys. Rev., **108**, 1175 (1957).
[15] Schwenk, A. et al., Nucl. Phys. A, **713**, 191 (2003).
[16] Takatsuka, T., Prog. Theor. Phys., **48**, 1517 (1972).
[17] Amundsen, L. et al., Nucl. Phys. A, **437**, 487 (1985a).
[18] Amundsen, L. et al., Nucl. Phys. A, **442**, 163 (1985b).
[19] Chen, J. M. C. et al., Nucl. Phys. A, **555**, 59 (1993)
[20] Kaminker, A. D et al., A& A, **373** 2 (2001).
[21] Ho, W. C. G. et al., Phys. Rev. C, **91**, 015806 (2015).
[22] Beznogov, M. V., Yakovlev, D. G., M.N.R.A.S., **447**, 2, 1598, 2015.
[23] Tsiopelas, S., Sagun, V., arXiv:2006.06351 [astro-ph.HE] (2020).

III. Cooling Processes & Gap models

The thermal evolution of NSs can be divided in two stages. During the first one, known as neutrino cooling era, ν_e emission generated from a plethora of emission mechanisms throughout the whole interior of the star dominates the cooling process [11, 12]. On a timescale of $\sim 10^6$ yrs after their formation, neutrino emission from the core has deteriorated enough so that photon emission from the surface overtakes as the leading heat loss mechanism, marking the start of the photon cooling era.

During the neutrino cooling era, the main factors regulating the neutrino emissivity of each process are density, temperature and the existing degree of Cooper pairing between particles. The composition of the envelope is another deciding factor for the surface photon luminosity of the star, which is ultimately the quantity of observational importance. In fact, heavier elements tend to delay heat transport from the outer crust to the surface, since in this case the electron thermal conductivity is reduced. In this work, we used two distinct envelope models: one composed of heavy elements (Fe) and a H-rich one that contains a fraction of light elements equal to $\eta = \Delta M/M = 10^{-7}$ [13].

Processes in core:

- Direct Urca $\qquad\qquad n \to pe\bar{\nu}_e\,,\ pe \to n\nu_e$;
- Modified Urca $\qquad\quad nN \to pNe\bar{\nu}_e\,,\ pNe \to nN\nu_e$;
- N-N Bremsstrahlung $\quad NN \to NN\nu\bar{\nu}$;
- e-p Bremsstrahlung $\quad ep \to ep\nu\bar{\nu}$.

Processes in crust:

- Pair annihilation $\qquad\quad ee^+ \to \nu\bar{\nu}$;
- Plasmon decay $\qquad\qquad \tilde{e} \to \tilde{e}\nu\bar{\nu}$;
- e-A Bremsstrahlung $\quad e(A,Z) \to e(A,Z)\nu\bar{\nu}$;
- n-n Bremsstrahlung $\quad nn \to nn\nu\bar{\nu}$.

Processes in both the crust and the core:

- Pair breaking-formation (PBF) $\quad \tilde{B} + \tilde{B} \to \nu\bar{\nu}$.

The most efficient neutrino-emitting processes taking place in the interior of the star are the direct Urca process of the neutron β-decay and its inverse. In general, the realization of these reactions depends on the proton fraction. For the IST EoS adopted in this work, they can occur in the core of stars with $n_c \geq 0.862\,fm^{-3}$ which translates to stars with a mass higher than $1.91\,M_\odot$. The effect originating from the onset of these reactions is visible in Figs. 5-7.
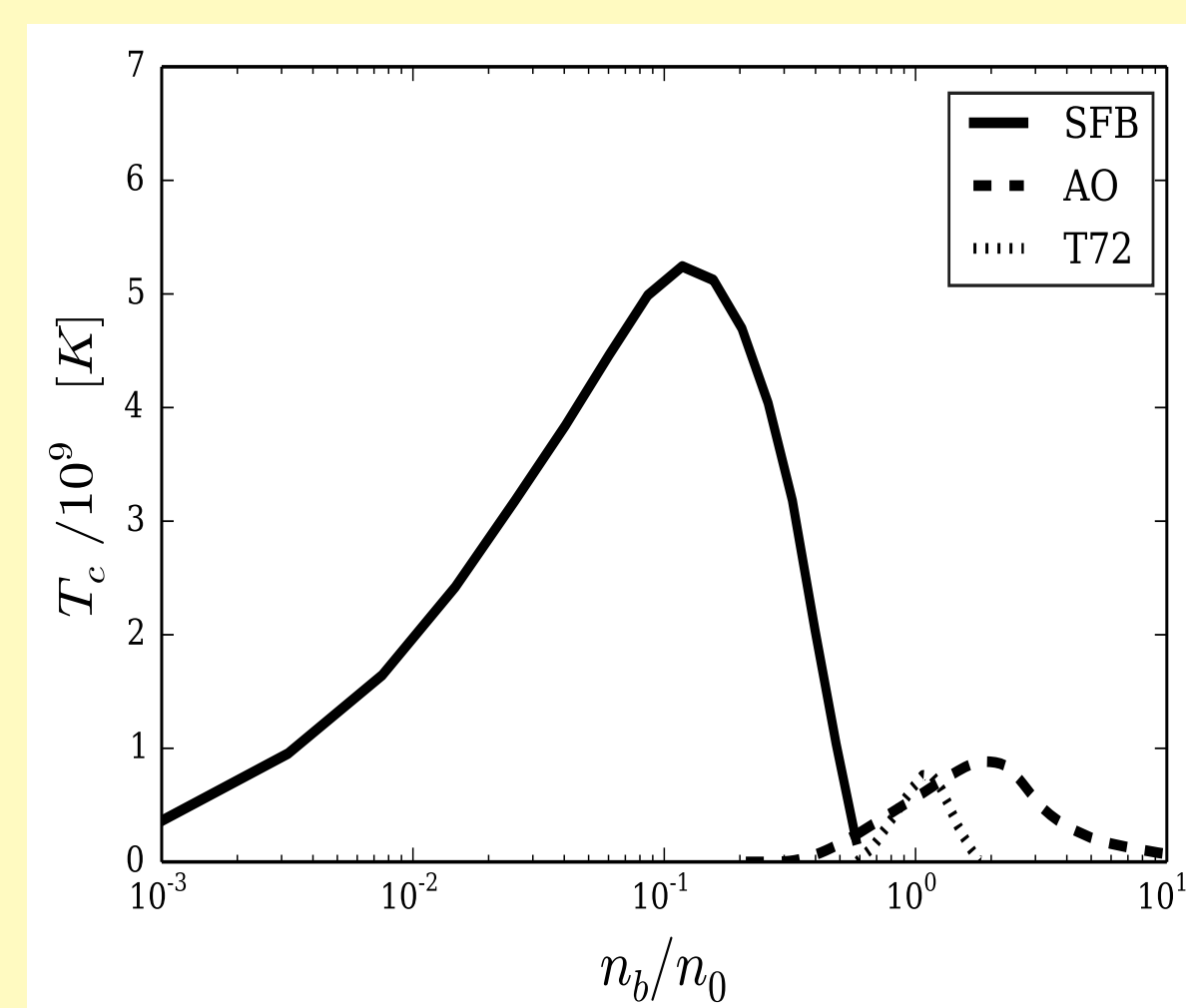

Fig.3. Density dependence of the critical temperature for the considered singlet and triplet neutron gaps.
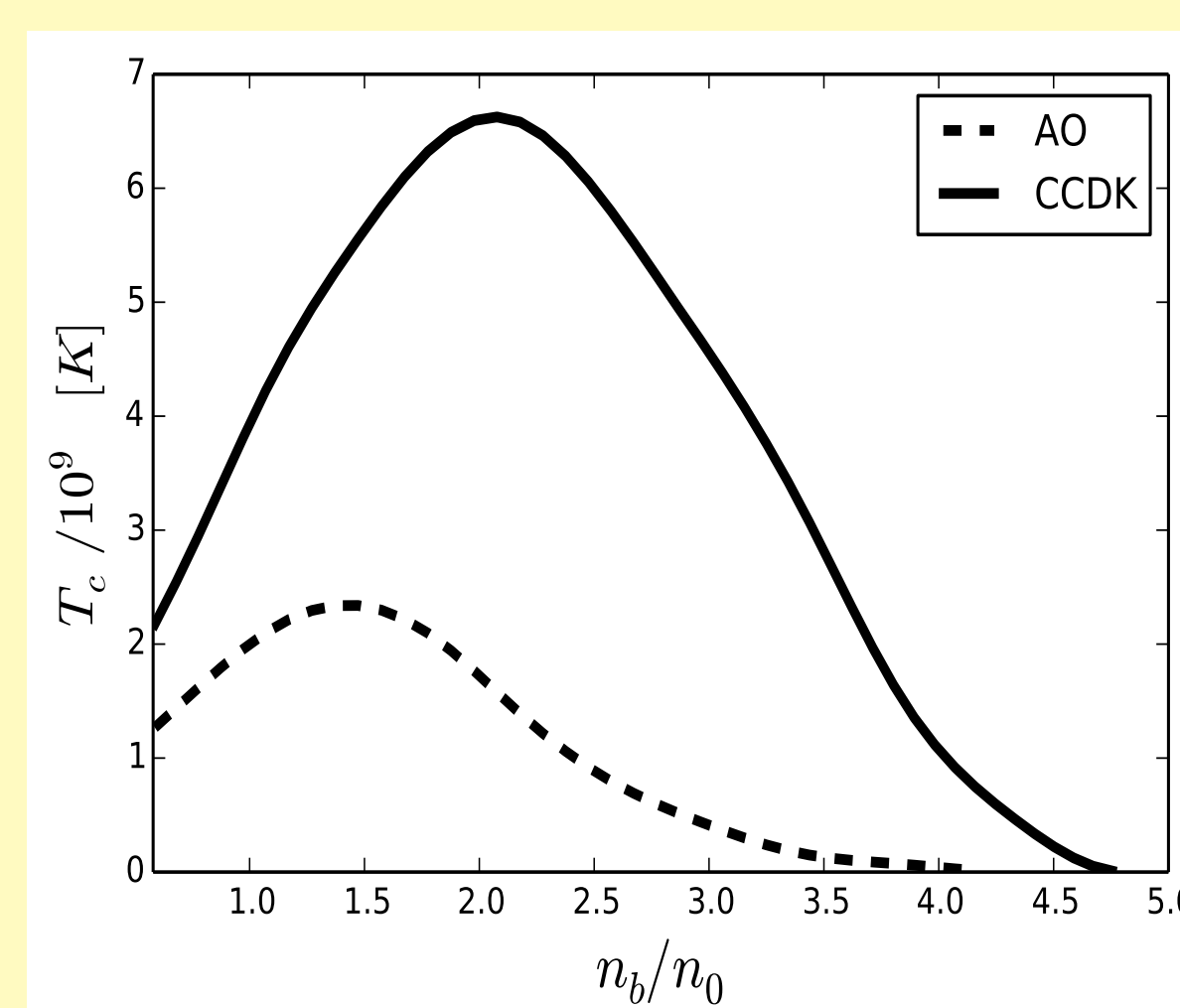

Fig.4. Density dependence of the critical temperature for the considered proton singlet pairing gaps.

Cooper pairing of core protons and crust neutrons sets in a few years after the NS birth, while core neutrons pairing is viable at a later time. All types of pairing follow the standards BCS pattern [14]. The onset temperatures $T_{c,n}(T_{c,p})$, the associated gap Δ and the profile of PBF neutrino emissivity vary over the several models developed to describe the paired matter. Our choice for the simulations were the following models: SFB [15] for the $^1S_0$ superfluidity of neutrons, T72 [16] and AO [17] for their $^3P_2$ superfluidity, and AO [18], CCDK [19] for the proton $^1S_0$ channel in different combinations. The critical temperatures T_c were calculated according to the phenomenological formula suggested by Kaminker et al. and the parameters used by Ho et al. [20, 21].
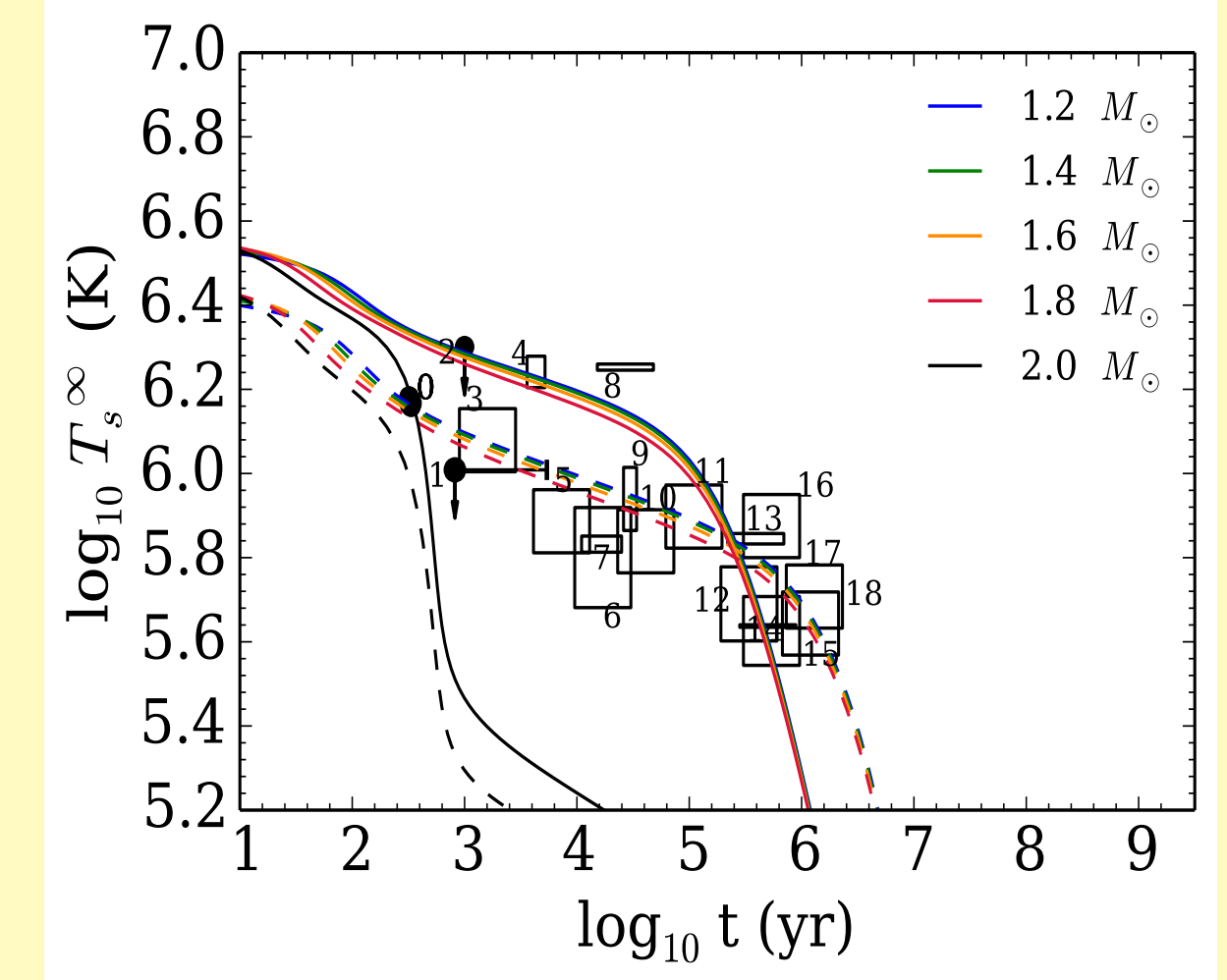
V. Results

Fig.5. Cooling curves for stars of different mass $M/M_\odot = 1.2, 1.4, 1.6, 1.8, 2.0$ for the case of unpaired matter. T_S^∞ denotes the surface temperature at infinity. Solid curves correspond to the light-element envelope ($\eta = 10^{-7}$), while dashed curves to the Fe envelope. The data points are taken from [22].
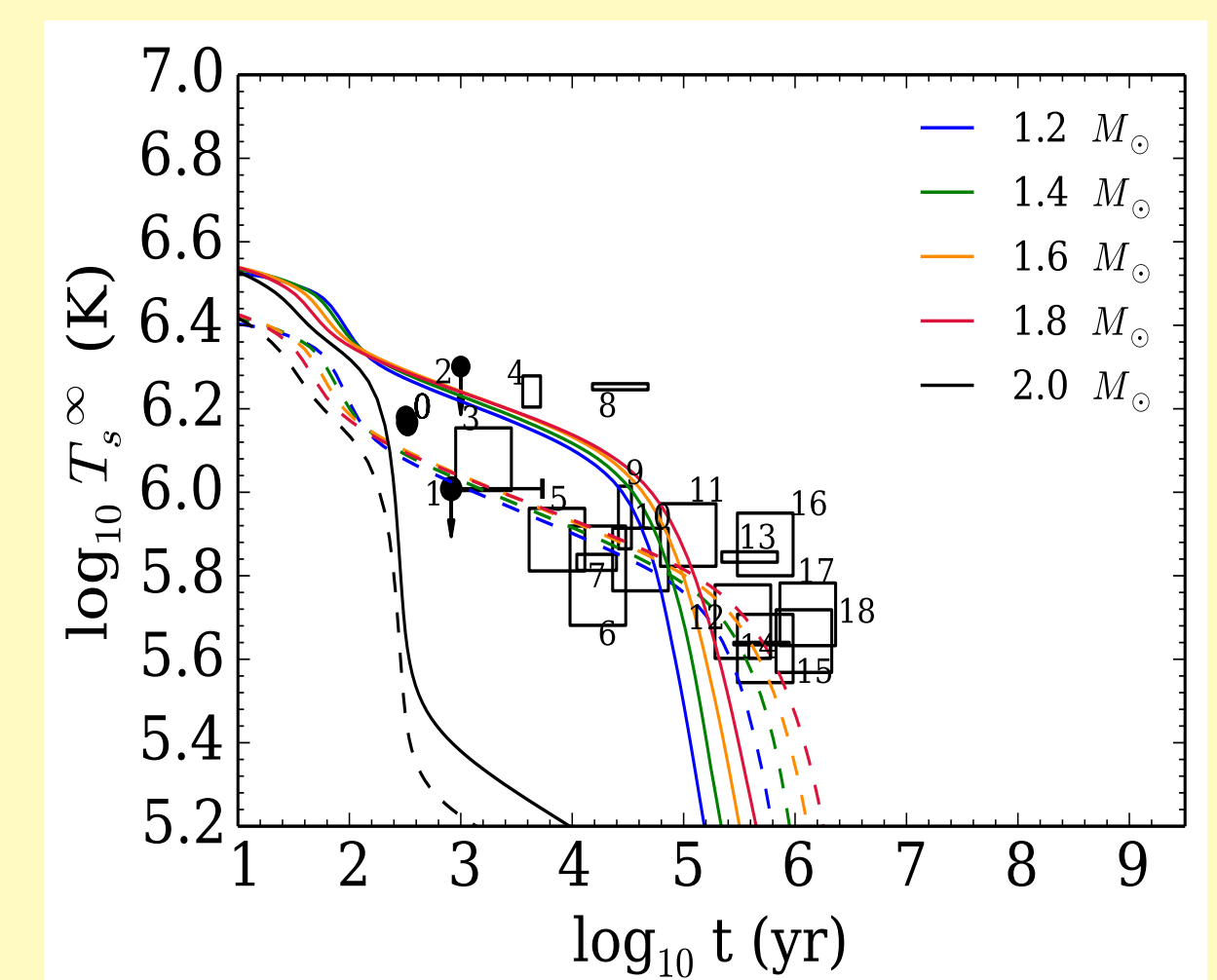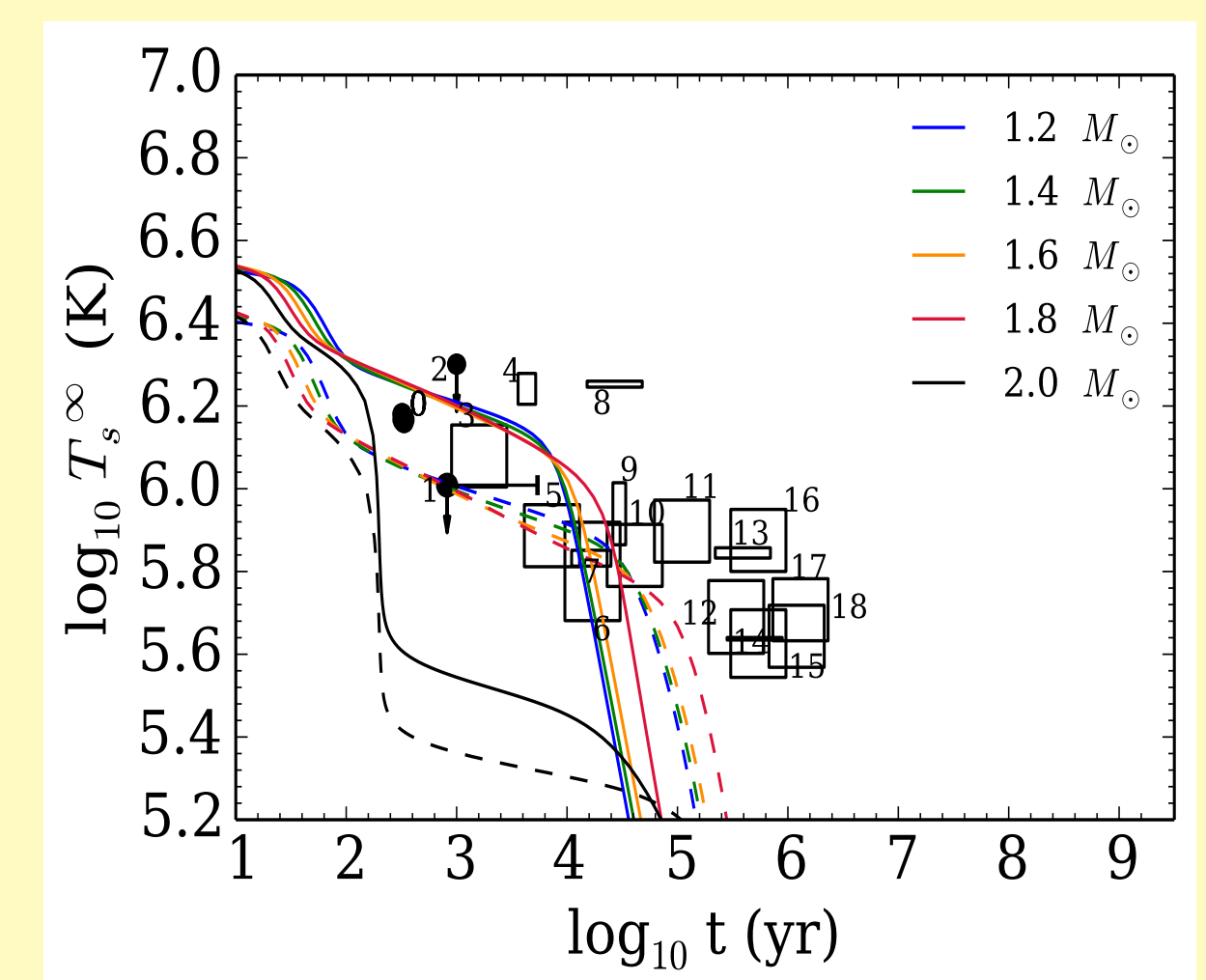

Fig.6. The same as Fig.5, but considering the effect of neutron superfluidity in the $^1S_0$ channel via the SFB model [15] and proton superconductivity in the $^1S_0$ channel with the AO model [17] (upper panel) and CCDK model [19] (lower panel).
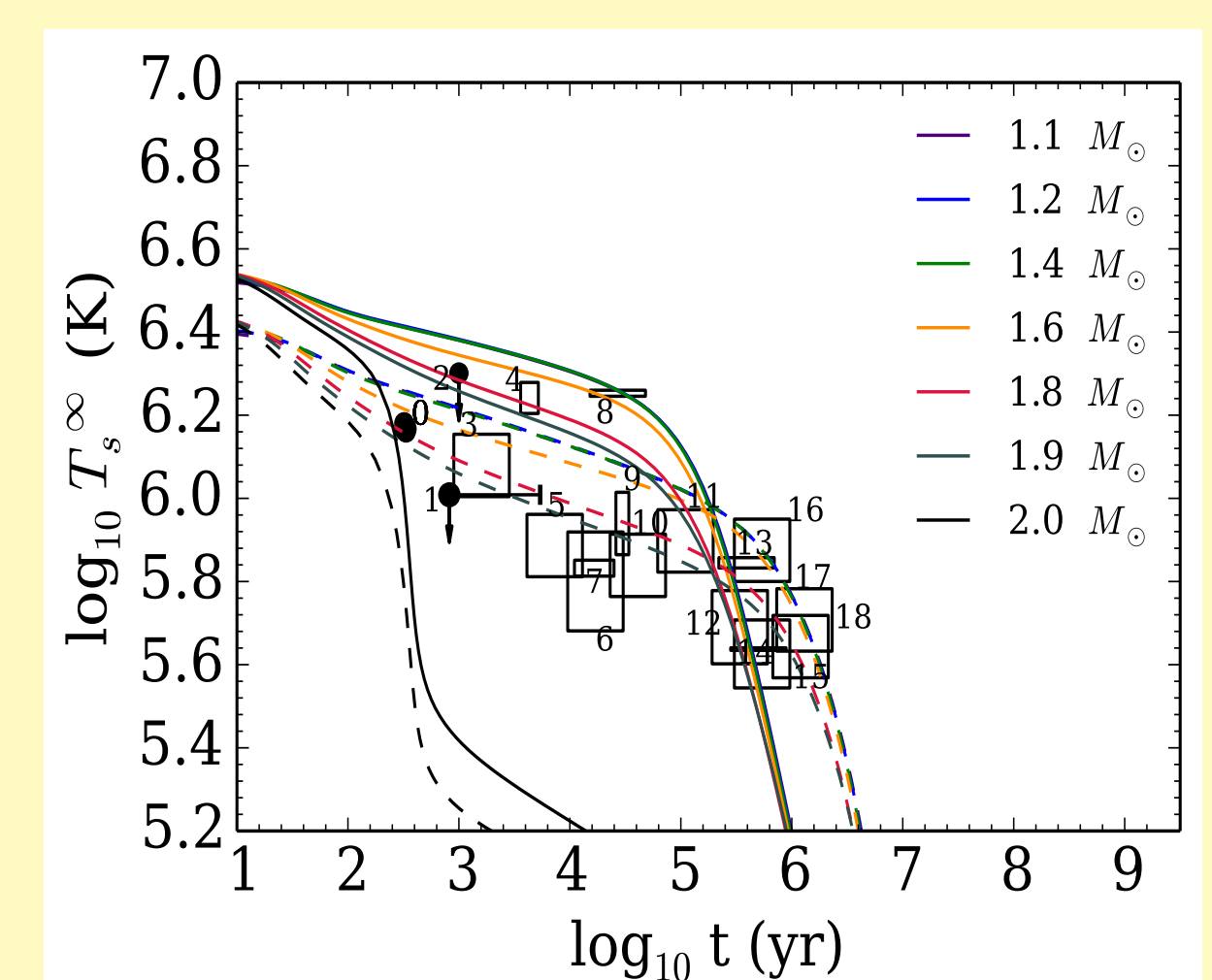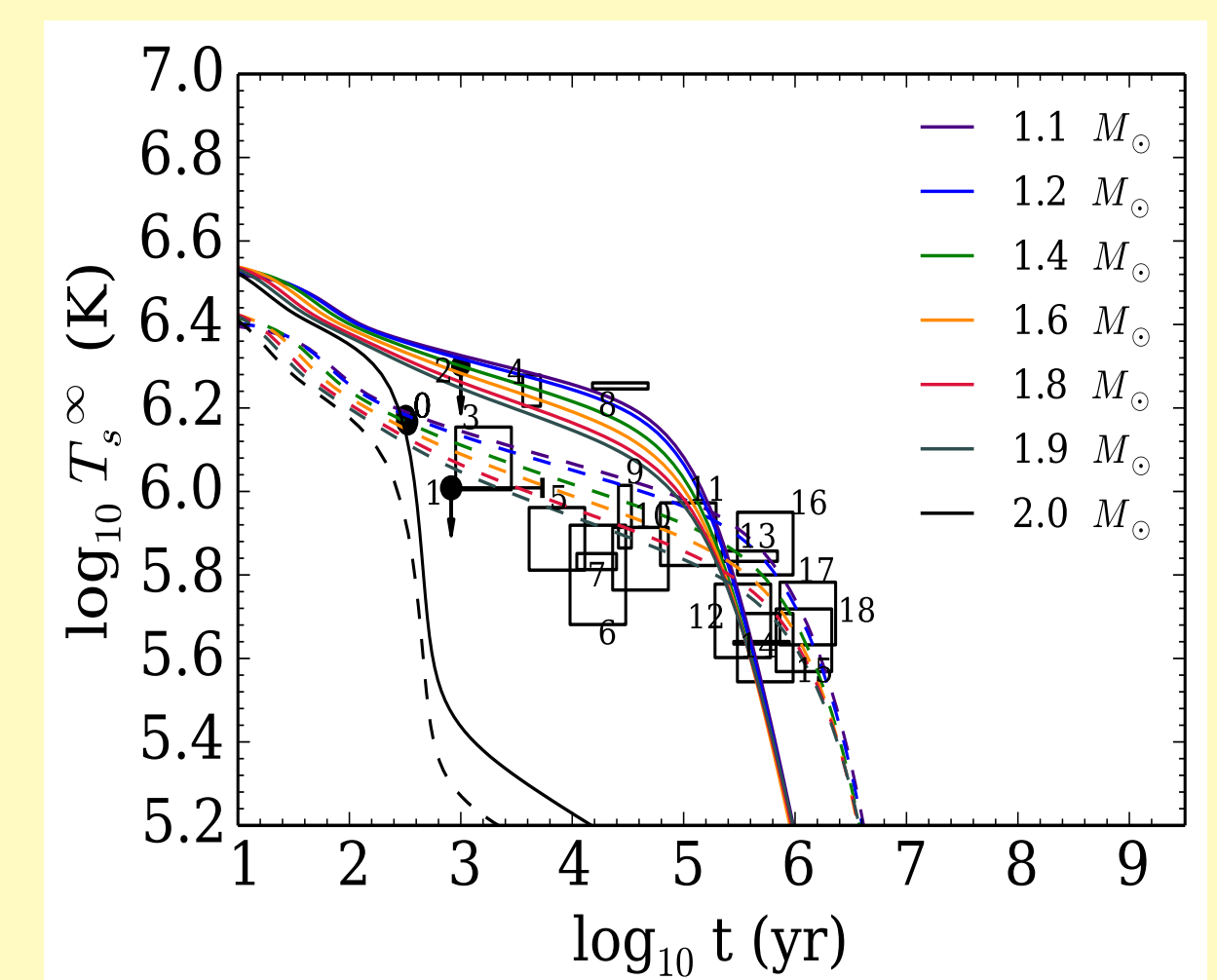

Fig.7. The same as lower panel of Fig.6, supplemented with the triplet neutron pairing in the core of the star described by the T72 model [16] (upper panel) and the AO model [18] (lower panel).

Modeling the thermal evolution of NSs was performed using the *NSCool* code [17, 18].

VI Conclusions

- The obtained cooling curves for unpaired matter (Fig.5) are in good agreement with observational data. The highly debatable NS of Cas A, noted as 0 on Figs. 5-7, can be equally described by both a rapidly cooling $2\,M_\odot$ star with a light-elements envelope and a slow cooling low-mass star with a Fe envelope [23].

- Including n $^1S_0$ superfluidity and p $^1S_0$ superconductivity in our simulations, we concluded that both considered combinations of gaps (SFB+AO, SFB+CCDK) result in cooling curves that are able to describe the observational data. In addition, the former one offers the same two ways of interpreting Cas A with the case of unpaired matter.

- Introducing n $^3P_2$ superfluidity in our calculations, using both a model with a shallow gap (T72) and one with an extended gap (AO), led to a more rapid cooling of the stars,. This rendered the obtained cooling curves incompatible with most of the observations, and thus neutron pairing in the triplet channel inconsistent with observational data within our model.